15TH IEA HEAT PUMP CONFERENCE
MAY 26–29, 2026 | HOFBURG
VIENNA 2026
DECARBONISATION THROUGH INNOVATION

A novel multi-scale hybrid physical and data-driven HVAC system model for optimal demand response control

Guo Yanhua[a], Shao Shuangquan[a,*], Chen Zhuang[a], Liang Yaran[a]

[a]School of Energy and Power Engineering, Huazhong University of Science and Technology, Wuhan 430074, China

Abstract

Model predictive control (MPC) of building HVAC systems plays a vital role in decarbonizing urban energy infrastructure, yet faces two fundamental implementation barriers: the degradation of data-driven model accuracy under small-sample regimes, and the computational intractability of physics-based models in real-time applications. Therefore, we present a multi-scale physics-data fusion (Ms-PDF) modeling framework and demonstrate its effectiveness in variable speed heat pump (VSHP) focused MPC tasks. In Ms-PDF, data-driven models are adopted at the component level and graph theoretic representations are used at the system level to support rapid collection and structuring of operational data. Building on this, a digital twin of the VSHP system is developed, which is integrated with a building thermal model to obtain a control-to-output dynamic thermal response model. Finally, a demand-responsive MPC controller is designed based on the derived thermal response model. Results demonstrate that the proposed Ms-PDF modeling platform achieves an average relative error of only 1.1%, and the digital-twin platform achieves up to 99.3% accuracy. With the developed MPC strategy, energy consumption and comfort-violation rate are reduced by 5.6%~20.7% and 28%~51%, respectively. These findings establish a new paradigm for interpretable hybrid modeling and provide a scalable pathway for deploying MPC in intelligent building systems.

Keywords: *Variable speed heat pump; Model predictive control; Data-driven; Energy Efficiency; Physics-Informed Neural Network*

1. Introduction

In HVAC systems, variable-speed heat pumps (VSHPs) have been widely used due to their high energy-efficiency and capability of providing grid frequency regulation without thermal storage [1,2]. VSHPs can effectively implement demand response (DR) strategies, including load shifting and load shedding [3], to reduce operational cost while maintaining thermal comfort based on advanced control like model predictive control (MPC) for output heating/cooling capacity regulation [4]. The implementation of MPC depends on the development of models for VSHPs, the building thermal dynamics, and the heating distribution system. While superior control performances of MPC based on TRNSYS or Modelica simulations have been validated by researchers, a long computation time of detailed model poses problems for field controllers [5]. Moreover, the reduced-order models based MPCs lead to significant differences between simulation results and actual values under partial load conditions. Therefore, it calls for balancing the modeling accuracy and computational efficiency [6].

Existing modeling approaches for VSHP systems mainly rely on data-driven methods, which require large and high-quality datasets [7, 8]. In practice, the available data are typically collected from historical operation, laboratory experiments, or simulations [9, 10]. Such data are often difficult to obtain flexibly and are costly in terms of time and labor. Moreover, if the system configuration changes, these models must be rebuilt by recollecting datasets, which limits their scalability and generalizability. Therefore, this study proposes a multi-scale physics-data fusion (Ms-PDF) modeling framework, aiming to conduct rapid data acquisition for VSHP systems with arbitrary configuration. Using the Ms-PDF framework, a digital twin of the VSHP system is

* Corresponding author. Tel.: 13051252727
E-mail address: shaoshq@hust.edu.cn

15th IEA Heat Pump Conference 2026 - ICO5.1 - https://doi.org/10.23697/saqc-r651

trained and further integrated with a building thermal model to construct a control to output dynamic thermal response platform. Finally, a short-term demand response MPC strategy is developed to obtain optimal control sequences for VSHP systems under real operating conditions.

2. Methodology

2.1. Construction of Ms-PDF framework

The physical modeling of VSHP systems relies on modular and hierarchical methods. Individual component models, such as compressors and heat exchangers, are first constructed. Subsequently, system-level nonlinear algebraic equations (AEs) are formulated based on the refrigerant flow sequence. However, replacing lumped-parameter models with distributed-parameter models to improve accuracy significantly increases the computational burden. Since component-level calculations consume most of the simulation time, replacing high-cost physical models with data-driven alternatives is a viable solution. Nevertheless, purely data-driven component models often lack the stability required for large-scale system simulations. To address these challenges, the Ms-PDF framework is developed (Fig. 1). It ensures scalability and construction efficiency by focusing on two key aspects: (1) constructing system models with strong physical consistency, and (2) enhancing the reliability of data-driven component models.

First of all, a general two-phase fluid network model is established based on the node-edge concept from graph theory, which can be applied to arbitrary system topologies, as shown in **Fig. 1 (a)**. Secondly, an exact and trend based physics-constrained neural network (ET-PCNN) is developed for each component which can be trained using exact physical laws rather than labeled data, resulting in higher construction efficiency, as shown in **Fig. 1 (b)**. Finally, the component models are coupled with the system-level fluid network to establish a set of nonlinear AEs, which are solved by the Newton-SOR algorithm, as shown in **Fig. 1 (c)**. The solving process incorporates equation formulation, newton-based iteration and relaxation strategy.

This simulation framework is adaptable to multiple ASHP configurations, including air-air, air-water, and water-water systems. Since the Ms-PDF formulates the heat pump system as a set of nonlinear algebraic equations derived from physical laws, it can, in principle, be applied to any working fluid (e.g., CO_2, R32), provided that the thermophysical property database is available. To test the effectiveness of the proposed framework, a multi-split (1-to-3) air-air source heat pump system operating in cooling mode is selected as the case study. The system includes three finned-tube evaporators, the variable-speed compressor and a configuration supporting the vapor-injection cycle.

To describe the connectivity between nodes and edges in a general manner, a node-edge incidence matrix $\boldsymbol{A}$ is introduced. For the two-phase fluid refrigerant network of the VSHP system shown in Fig. 1(a), the matrix $\boldsymbol{A}$ can be expressed as Eq. (1).

$$\mathbf{A}=\begin{bmatrix} -1 & 1 & 0 & 0 & \cdots & a_{1,j} & \cdots & 0 \\ 0 & 0 & 1 & 0 & \cdots & a_{2,j} & \cdots & 0 \\ 1 & 0 & 0 & -1 & \cdots & a_{3,j} & \cdots & 0 \\ 0 & -1 & 0 & 0 & \cdots & a_{4,j} & \cdots & 0 \\ \vdots & \vdots & \vdots & \vdots & \ddots & \vdots & \vdots & \vdots \\ a_{i,0} & a_{i,1} & a_{i,2} & a_{i,3} & \cdots & a_{i,j} & \cdots & a_{i,N_B} \\ \vdots & \vdots & \vdots & \vdots & \vdots & \vdots & \ddots & \vdots \\ 0 & 0 & 0 & 0 & \cdots & a_{N_N,j} & \cdots & -1 \end{bmatrix}, \tag{1}$$

$$\text{where} \quad a_{i,j}=\begin{cases} 1 & \text{node } i \text{ is inlet of edge } j; \\ -1 & \text{node } i \text{ is outlet of edge } j; \\ 0 & \text{else.} \end{cases}$$

We define the entries $a_{i,j}=1$ in the $\boldsymbol{A}$ as the inlet incidence matrix, denoted by $\boldsymbol{A_I}$, and $a_{i,j}=-1$ as the outlet incidence matrix, denoted as $\boldsymbol{A_O}$. It should be noted that the rank of the $\boldsymbol{A}$ is N_N-1. Therefore, a full-rank base node-edge incidence matrix $\boldsymbol{A_B}$ can be obtained by removing any one row of $\boldsymbol{A}$. By combining $\boldsymbol{A_B}$ with the mass and energy conservation equations at each node, the refrigerant flow distribution and thermodynamic state can be fully described by Eq. (2), (3), and (4).

$$\text{Mass flow: } \boldsymbol{A_B R}=0 \tag{2}$$

$$\text{Energy: } \boldsymbol{A_O}(\boldsymbol{RH_O}) - \boldsymbol{A_I}(\boldsymbol{RH_I}) = \boldsymbol{0}; \boldsymbol{H_I} = \boldsymbol{A_I^T H} \tag{3}$$

$$\text{Momentum: } \boldsymbol{P_O} - \boldsymbol{A_O^T P} = \boldsymbol{0} \tag{4}$$

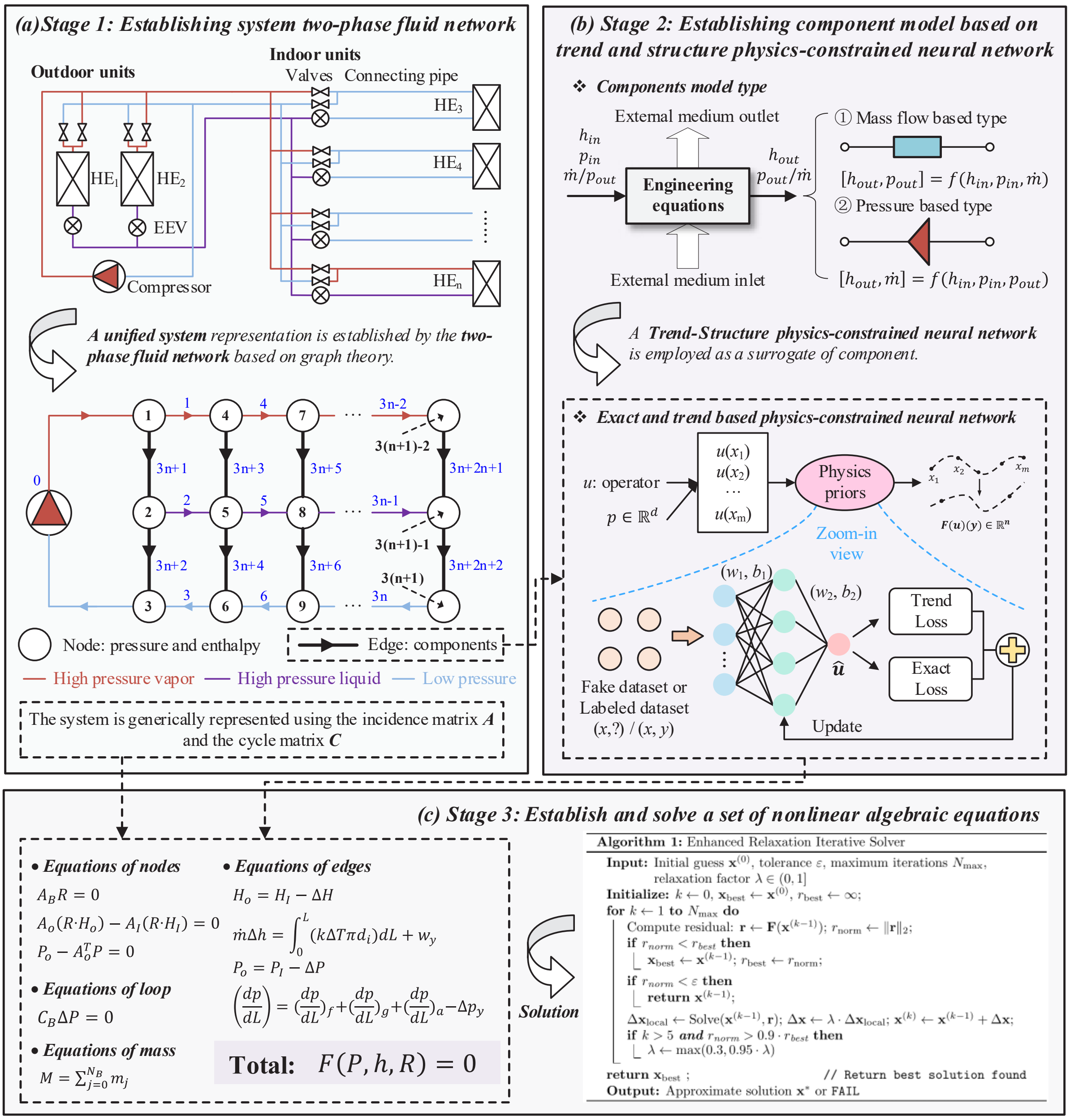

Figure 1. Flowchart of the proposed Ms-PDF modeling framework.

A loop matrix $\boldsymbol{C}$ is introduced to represent the combination of edges within each closed loop, ensuring that pressure conservation is satisfied along every loop, as illustrated in Eq. (5) and (6).

$$\mathbf{C} = \begin{bmatrix} 1 & 0 & 0 & 0 & \cdots & c_{1,j} & \cdots & 0 \\ 0 & 1 & -1 & 0 & \cdots & c_{2,j} & \cdots & 0 \\ 0 & 0 & 1 & 1 & \cdots & c_{3,j} & \cdots & 0 \\ 0 & 0 & 0 & 0 & \cdots & c_{4,j} & \cdots & 0 \\ \vdots & \vdots & \vdots & \vdots & \ddots & \vdots & \vdots & \vdots \\ c_{i,0} & c_{i,1} & c_{i,2} & c_{i,3} & \cdots & c_{i,j} & \cdots & c_{i,N_B} \\ \vdots & \vdots & \vdots & \vdots & \vdots & \vdots & \ddots & \vdots \\ 0 & 0 & 0 & 0 & \cdots & c_{N_N,j} & \cdots & 1 \end{bmatrix}, \tag{5}$$

where $c_{i,j} = \begin{cases} 1 & \text{if edge } j \text{ is in circuit } i \text{ and orientations of the circuit and the edge coincide;} \\ -1 & \text{if edge } j \text{ is in circuit } i \text{ and orientations of the circuit and the edge are opposite;} \\ 0 & \text{if edge } j \text{ is not in circuit } i. \end{cases}$

$$\text{Cycle:} \quad \boldsymbol{C_B}(\boldsymbol{P_I} - \boldsymbol{P_O}) = 0; \boldsymbol{P_I} = \boldsymbol{A_I^T P}, \tag{6}$$

In addition, VSHP systems must also satisfy system-level mass conservation. For a system with a specified refrigerant charge, the mass conservation condition can be expressed as:

$$\text{Mass:} \quad M = \sum_{j=0}^{N_B} m_j, \tag{7}$$

where M is the total refrigerant charge. m_j is the refrigerant charge of edge N_j.

In the calculation process, $\boldsymbol{P}$, $\boldsymbol{H}$, $\boldsymbol{R}$ are usually initialized, and to evaluate the above equations, $p_{O,j}$, $h_{O,j}$, and m_j of each edge N_j must be known. Determining these quantities requires knowledge of the heat transfer and flow characteristics of the components along each edge. Therefore, it is necessary to further develop detailed component models.

2.2. Digital twin of VSHPs and thermal model

With the Ms-PDF platform, a large amount of operational data can be efficiently generated. Based on this ability, we design a novel training algorithm, as shown in **Fig. 2**, namely cross-scale physics-informed neural network (CS-PINN). The overall training process begins by feeding fake datasets into the system-level solver network to produce predicted outputs. The loss function is then computed and propagated backward along the multi-layer structure. The compressor model is selected as the starting point for each computational loop within the system-level graph. To achieve stable optimization, a hybrid optimizer combining Adam and L-BFGS is employed.

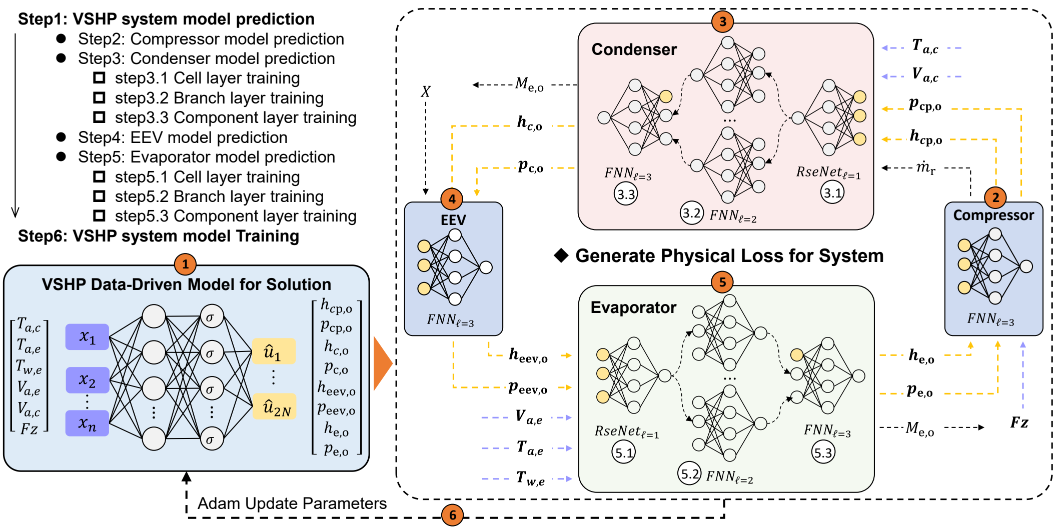

Figure 2. Training strategy for the digital twin of the VSHP system.

The trained VSHP model can predict specific enthalpy and pressure at each node according to disturbance and control inputs. In control applications, system performance metrics are of greater interest. Thus, we convert the model outputs into key performance indicators, namely the cooling capacity (Q_c) and coefficient of performance (COP). These are derived based on thermodynamic relations:

$$Q_c = \dot{m}_r \cdot (h_{e,o} - h_{e,i}) \tag{8a}$$

$$COP = \frac{Q_c}{P_{comp}}, \tag{8b}$$

where $h_{e,o}, h_{e,i}$ represent the refrigerant enthalpy at the outlet and inlet of the evaporator, respectively. P_{comp} denotes the compressor power. the trained VSHP model for performance prediction can be expressed as:

$$[Q_c, COP, P_{comp}] = F(T_{a,out}; T_{a,in}; T_{s,in}; V_{a,e}; V_{a,c}; Fz), \tag{9}$$

where $T_{a,out}$ is the condenser inlet air dry bulb temperature. $T_{a,in}, T_{s,in}$ are the evaporator inlet air dry and wet bulb temperatures. $V_{a,e}, V_{a,c}$ denote the air volume flow rates on the evaporator and condenser sides, and Fz is the compressor frequency.

The control-oriented thermal response of the VSHP can be represented by a general discrete-time nonlinear state-space model, as defined by:

$$\boldsymbol{x}(k) = f(\boldsymbol{x}(k-1), \boldsymbol{u}(k-1), \boldsymbol{d}(k-1)) \tag{10a}$$

$$\boldsymbol{y}(k) = F(\boldsymbol{x}(k), \boldsymbol{u}(k), \boldsymbol{d}(k)), \tag{10b}$$

where the vectors $\boldsymbol{x}, \boldsymbol{u}, \boldsymbol{d}, \boldsymbol{y}$ denote the system state, control input, external disturbance, and model output, respectively. Specifically:

$$\boldsymbol{x}(k) = [T_1(k); T_2(k); T_m(k); T_a(k); T_{w,e}(k)]^T \in \mathbb{R}^5 \tag{11a}$$

$$\boldsymbol{u}(k) = [V_{a,e}(k); V_{a,c}(k); Fz(k)]^T \in \mathbb{R}^3 \tag{11b}$$

$$\boldsymbol{d}(k) = [T_{out}(k); Q_{sol}(k); Q_{ihg}(k)]^T \in \mathbb{R}^3 \tag{11c}$$

$$\boldsymbol{y}(k) = [COP(k); Q_c(k)]^T \in \mathbb{R}^2, \tag{11d}$$

where T_1, T_2, T_m are the temperatures at internal virtual nodes in the building resistance-capacitance (RC) model, respectively. T_a, $T_{w,e}$ are the indoor air dry bulb and wet bulb temperatures, respectively. T_{out} is the outdoor air dry bulb temperature. Q_{sol}, Q_{ihg} represent the solar radiation and internal heat gains, respectively. The functions $f(\cdot), F(\cdot)$ denote the nonlinear state-space and output functions, respectively. As shown in **Fig. 3**, the indoor temperature controller serves as the interface linking the VSHP model and the thermal response model of the room. Based on the real-time indoor temperature feedback, the controller determines the appropriate compressor frequency for the next time step. Given the selected compressor frequency and the disturbance inputs, the VSHP model predicts the corresponding cooling capacity and COP. These outputs are following passed into the room thermal model to compute the indoor air temperature and temperatures of virtual thermal nodes at the subsequent time step. It is worth noting that, in this study, the fan speeds for the evaporator and condenser are fixed.

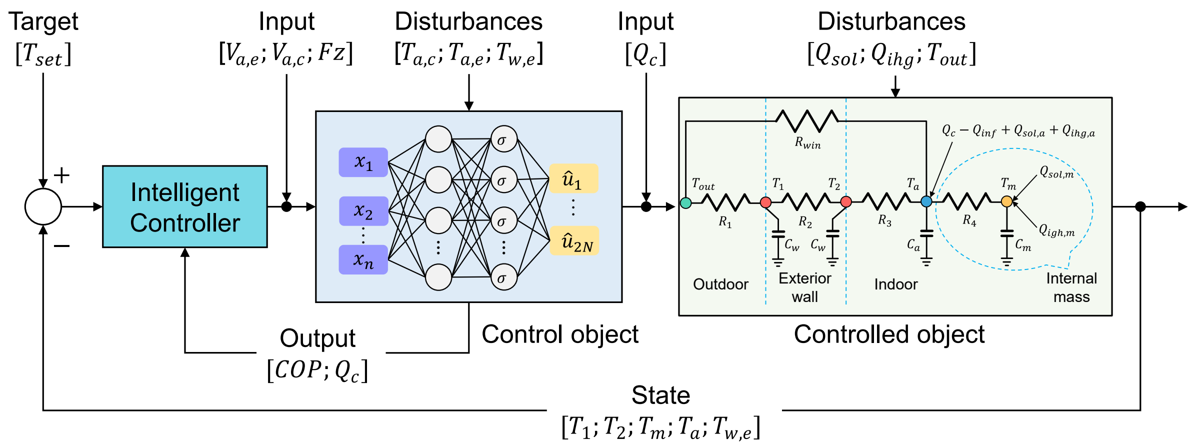

Figure 3. Thermal response process of the VSHP and room model for control.

2.3. MPC control strategy

As shown in **Fig. 4**, this study designs two types of control variables: indoor temperature setpoint schedule (updated hourly) and compressor frequency (updated every 5 minutes). These two layers are a rolling optimization framework, where the upper-level optimizer determines the setpoint schedule for the entire day, and the lower-level optimizer provides real-time compressor frequency.

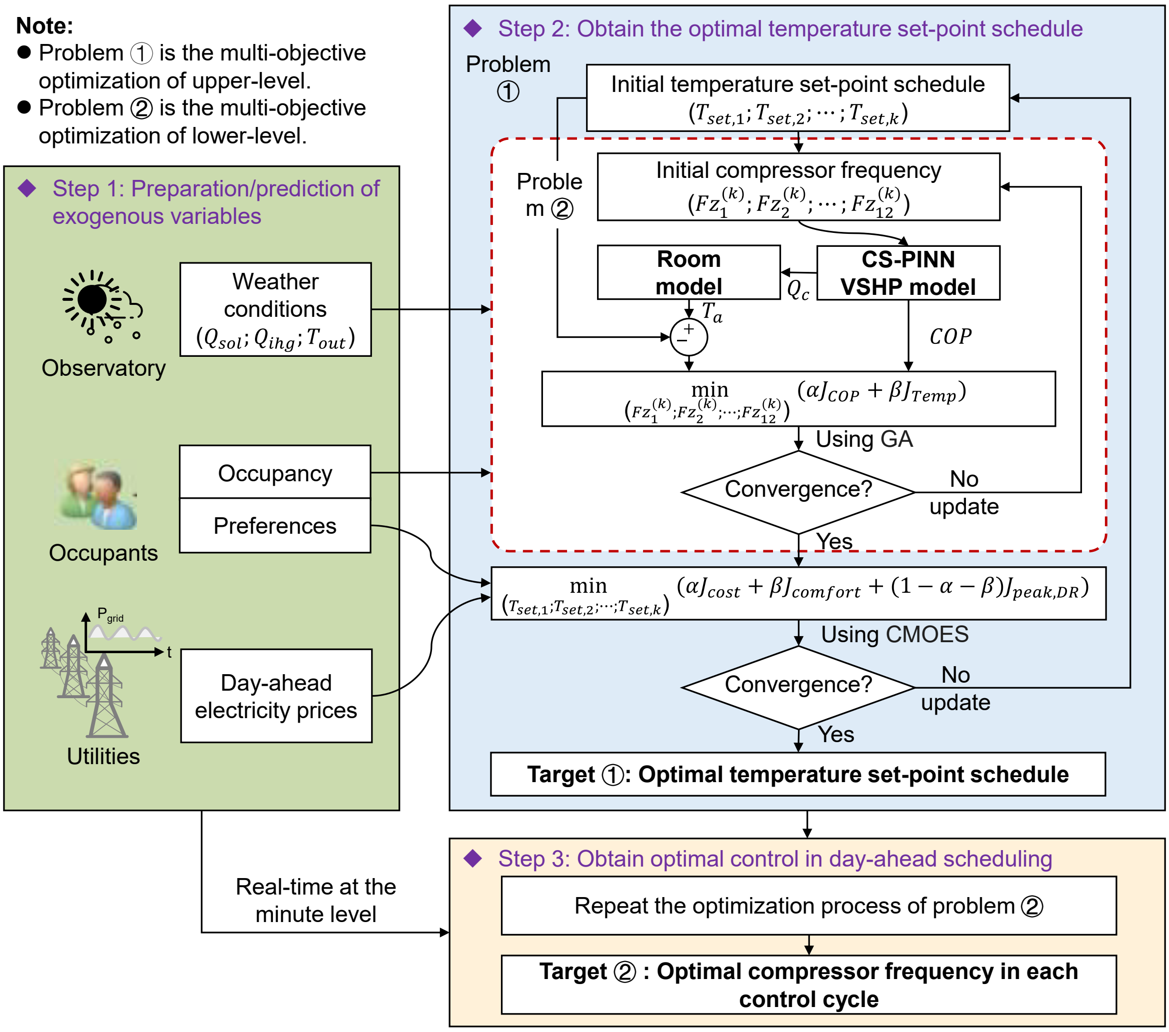

Figure 4. Model-based optimal control method framework.

The upper-level optimization aims to achieve a multi-objective trade-off among thermal comfort, electricity cost, and peak demand reduction during demand response (DR) periods. The cost function is defined as:

$$\min_{(T_{set,1}; T_{set,2}; \cdots; T_{set,k})} (\alpha J_{cost} + \beta J_{comfort} + (1-\alpha-\beta) J_{peak,DR}) \\ s.t. T_{set,lb} \leq T_{set,k} \leq T_{set,ub}, \tag{12}$$

where thermal comfort cost ($J_{comfort}$) quantified by the predicted mean vote (PMV) deviation; electricity cost (J_{cost}) as the product of hourly energy consumption and hourly electricity prices; peak demand cost ($J_{peak,DR}$) representing the maximum compressor power during DR windows:

$$J_{comfort} = PMV_{bd} - F_{PMV}(T_{a,k}, T_{w,e,k}) \tag{12a}$$

$$J_{cost} = \sum_{i=1}^{m} E_i C_i \tag{12b}$$

$$J_{peak,DR} = max\{P_1; P_2; \cdots; P_l\} \tag{12c}$$

Given that hourly temperature setpoints directly affect indoor thermal response and energy performance, a fine-grained compressor frequency optimization is performed at the lower level to support upper-level decision-making. The lower-level cost function simultaneously minimizes temperature deviation and maximizes instantaneous system efficiency (COP). The objective of using instantaneous COP in the optimization process is to ensure that the system maintains its optimal operational state at each time step throughout the rolling horizon.

$$\min_{(Fz_1^{(k)};Fz_2^{(k)};\cdots;Fz_{12}^{(k)})} (\alpha J_{COP} + \beta J_{Temp}) \tag{13}$$

$$J_{Temp} = \sqrt{\frac{1}{n}\sum\nolimits_{j=1}^{n}(T_{a,j} - T_{set,j,k})^2} \tag{13a}$$

$$J_{COP} = \frac{1}{n}\sum_{i=1}^{n} COP_j \tag{13b}$$

3. Results and Discussion

3.1. Validation of Ms-PDF framework

The trained component-level ET-PCNN, convolutional neural network (CNN), long short-term memory (LSTM), and random forest (RF) models are integrated into the Ms-PDF for system-level solution. A typical solving process is shown in **Fig. 5**. For ET-PCNN component-level models, the iterative solver converges rapidly to a tolerance of 1×10^{-6}, similar to PM method. In contrast, the CNN and LSTM component-level models tend to cause oscillatory behavior during the system-level iterative solution. It is evident that purely data-driven models cannot faithfully capture key physical trends. Repeated tests show that CNN and LSTM models typically converge to 1×10^{-4} and fail to reach the stricter tolerance of 1×10^{-6}. The RF model, although achieving more than 90% accuracy at the component level, performs even worse during system-level solving.

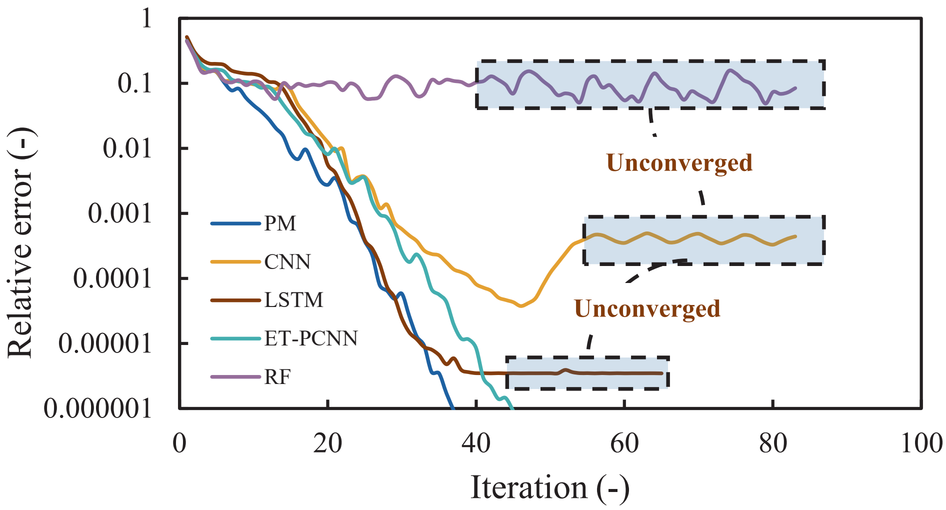

Figure 5. Typical convergence process using different data-driven component models.

For a vapor compression system, evaporating pressure, condensing pressure, and the Coefficient of Performance (COP) are critical indicators. As shown in **Fig. 6**, the ET-PCNN achieves the best system-level performance with no significant bias. The Mean Relative Errors (MREs) for condensing pressure, evaporating pressure, and COP are 1.1%, 0.9%, and 0.8%, respectively. Conversely, CNN and LSTM models show larger deviations. For instance, the CNN model exhibits increased prediction bias as condensing pressure rises, indicating inaccuracies in the condenser sub-model. These results confirm that ET-PCNN, by incorporating physical trend constraints, enhances both prediction accuracy and stability.

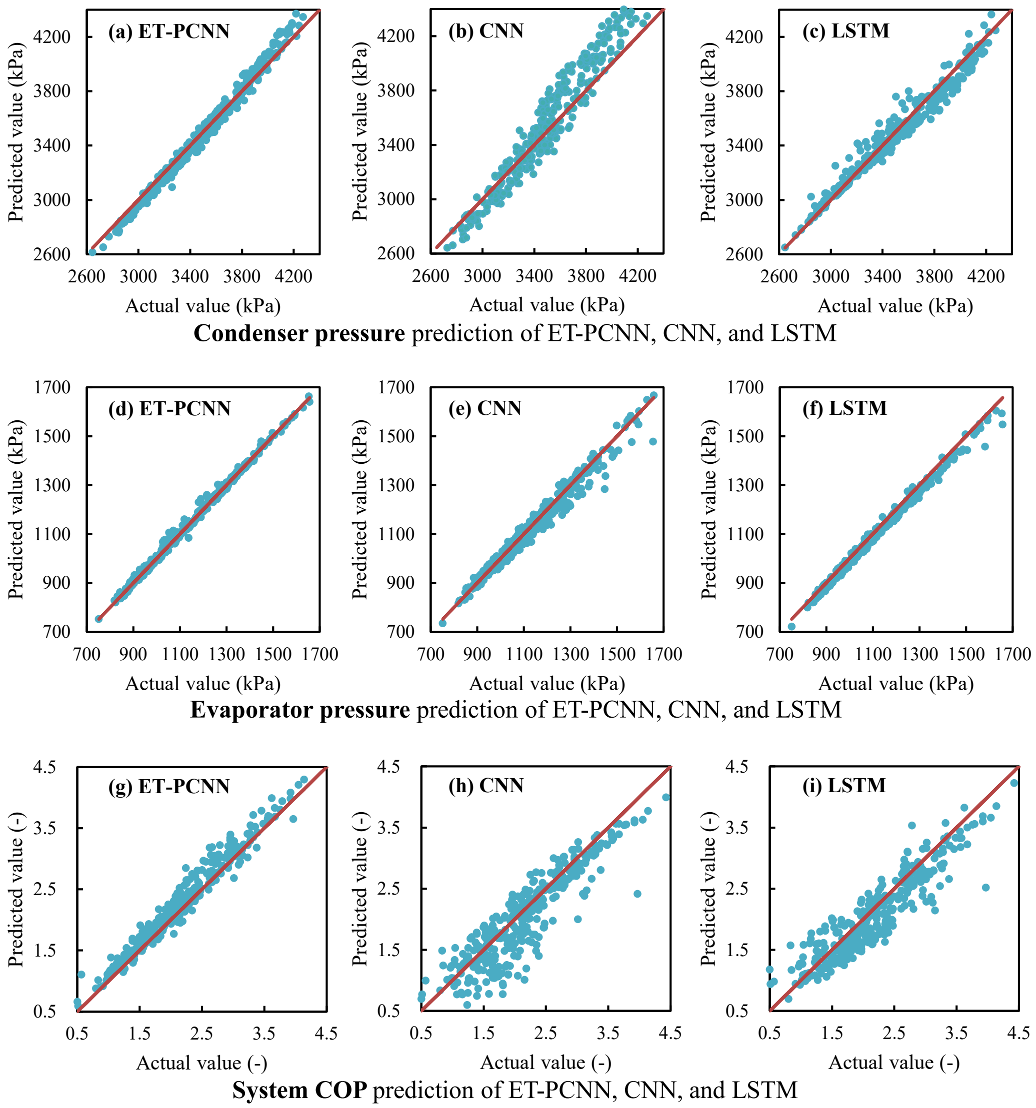

Figure 6. System-level simulation performance of different component models under test operating conditions.

3.2. Validation of digital twin for the VSHP

To validate the CS-PINN, we generated a dataset comprising 2,200 labelled samples using Latin Hypercube Sampling method employed the validated Ms-PDF physical model. Of the full dataset, 80% is allocated for training, 10% for validation, 10% for testing. The variables ranges are summarized in Table 1.

Table 1 Variable ranges in the selected dataset.

Variables		**Ranges ([start, end])**	**Units**
Input features	Compressor frequency (Fz)	[30, 110]	Hz
	Outdoor air dry-bulb temperature (T_{out})	[22, 38]	℃
	Indoor air dry-bulb temperature (T_a)	[20, 30]	℃
	Indoor relative humidity (Rh)	[20, 80]	%
	Air volume flow rate of condenser ($V_{a,c}$)	[1600, 3400]	m^3/h
	Air volume flow rate of evaporator ($V_{a,e}$)	[600, 1800]	m^3/h
Outputs	Cooling capacity (Q_c)	[2.12, 9.11]	kW
	Compressor power (P_{comp})	[0.58, 3.57]	kW
	Operational efficiency (COP)	[1.59, 5.91]	–

Table 2 summarizes the predicted performance of different models on the test dataset. The CS-PINN exhibits the highest prediction accuracy across various VSHP system performance indicators, achieving R^2 values of 0.999, 0.996, and 0.993 for compressor power, cooling capacity, and COP, respectively. The multi-

Layer perceptron (MLP) ranks second, followed by LSTM, while CNN shows the weakest performance. Due to the relatively small distribution shift between the training and test datasets, all purely data-driven models still deliver reasonably good results overall. To further evaluate prediction robustness, the absolute errors of each model's predictions are categorized into five intervals, as illustrated in **Fig. 7.** It is evident that the majority of CS-PINN's predictions for compressor power, cooling capacity, and COP fall within the ±5% error range. CNN exhibits maximum errors exceeding ±20%. Results highlight the superior robustness and generalization capability of the CS-PINN, ensuring consistent prediction accuracy under small-sample constraints.

Table 2. Performance of different models on the test dataset.

Model	**Q_c prediction**			**P_{comp} prediction**			**COP prediction**		
	MAE	RMSE	R^2	MAE	RMSE	R^2	MAE	RMSE	R^2
CS-PINN	**0.027**	**0.035**	**0.999**	**0.041**	**0.046**	**0.996**	**0.059**	**0.065**	**0.993**
MLP	0.087	0.12	0.992	0.044	0.061	0.993	0.059	0.078	0.989
CNN	0.14	0.19	0.978	0.059	0.079	0.988	0.078	0.11	0.982
LSTM	0.10	0.13	0.990	0.049	0.041	0.992	0.061	0.091	0.986

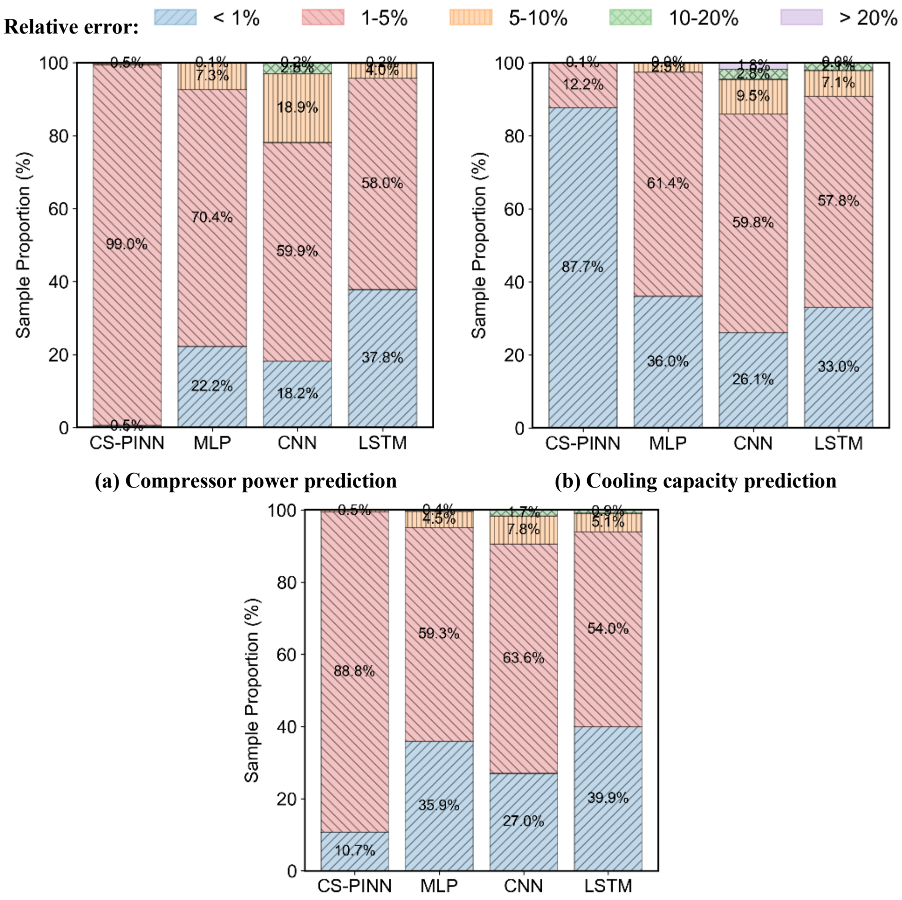

(c) COP prediction

Figure 7. Validation of the trained digital twin for VSHP.

3.3. Validation of digital twin for VSHPs and thermal mass model

Fig. 8 compares various control strategies: PID, MLP-based MPC, CNN-based MPC, LSTM-based MPC, and the proposed CS-PINN-based MPC. **Fig. 8(a)** and **Fig. 8(b)** illustrate the distributions of the Temperature Difference (TD) and the Predicted Mean Vote (PMV), respectively. The CS-PINN-based MPC achieves the best comfort, with an average TD of 0.36 K and an average PMV of 0.44. Compared to MLP, CNN, LSTM, and PID, the CS-PINN increases the comfort-maintaining time by 28%, 51%, 34%, and 38%, respectively. Furthermore, it reduces energy consumption by up to 20.7% compared to CNN-based MPC (**Fig. 8c**).

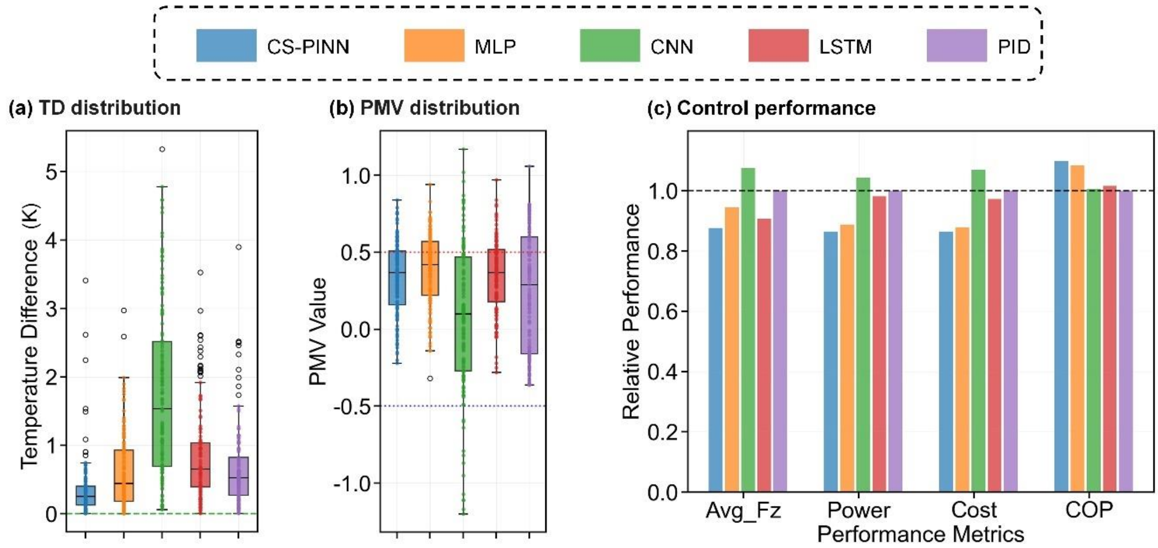

Figure 8. Comparative control performance of different models.

Furthermore, **Fig. 9** illustrates the temperature control performance and energy consumption profiles of five controllers operating from 8:00 to 18:00: CS-PINN-based MPC (a), MLP-based MPC (b), CNN-based MPC (c), LSTM-based MPC (d), and the conventional PID controller (e). The purple line represents the indoor temperature trajectory, while the black dashed line indicates the setpoint. The orange and green bars denote the cooling capacity and compressor power consumption, respectively. Intuitively, the closer the purple line is to the setpoint, the better the temperature regulation. Smaller average temperature difference (ATD) implies reduced temperature fluctuations, which in turn help minimize unnecessary power consumption. To provide a quantitative comparison of the control stability, the average absolute change of frequency (AACF) is calculated for each method to measure the fluctuations in control actions. The CS-PINN-based MPC achieves the lowest frequency fluctuation with an AACF of 20.47, while the MLP, CNN, and LSTM models exhibit significantly higher fluctuations of 31.57, 27.87, and 26.68, respectively. Hence, the CS-PINN-based MPC controller demonstrates superior performance, maintaining more stable temperature tracking and smoother power curves. In contrast, other controllers, particularly the CNN-based MPC, exhibit more significant fluctuations in power consumption, indicating unstable compressor frequency adjustments, which is not desirable in real-world operation. The CNN-based controller performs worse than the PID controller in certain instances, highlighting the importance of physical consistency in prediction-based control.

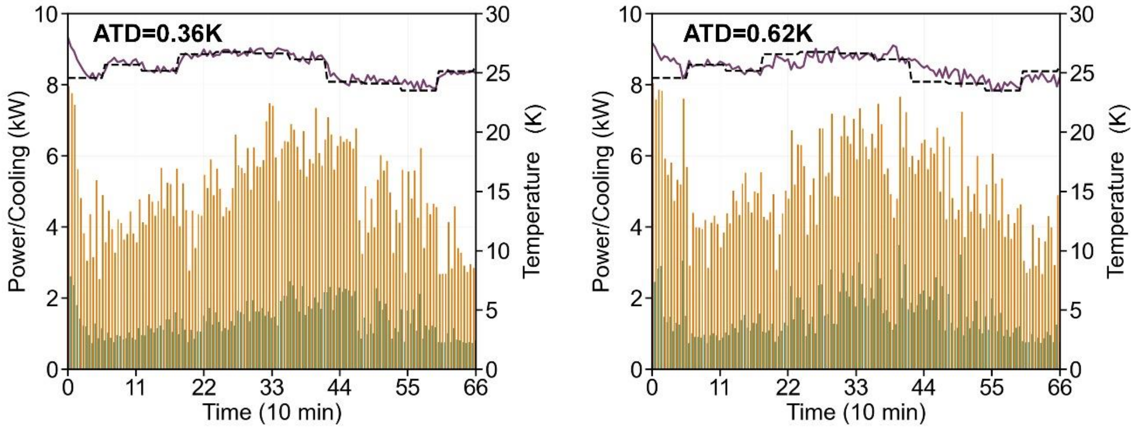

(a) CS-PINN based MPC **(b) MLP based MPC**

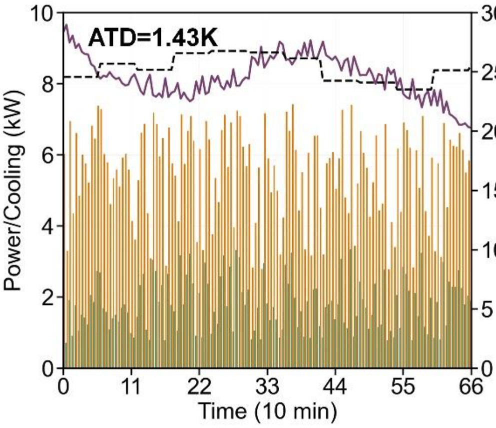

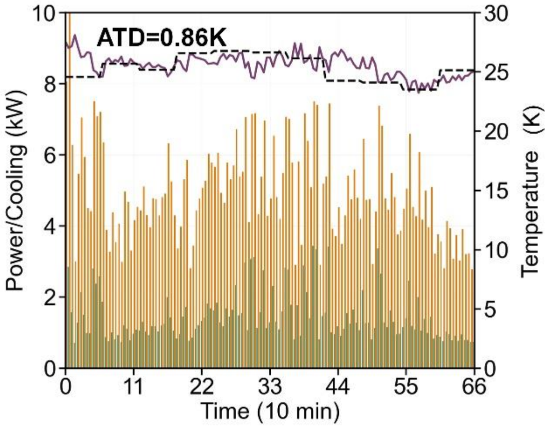

(c) CNN based MPC **(d) LSTM based MPC**

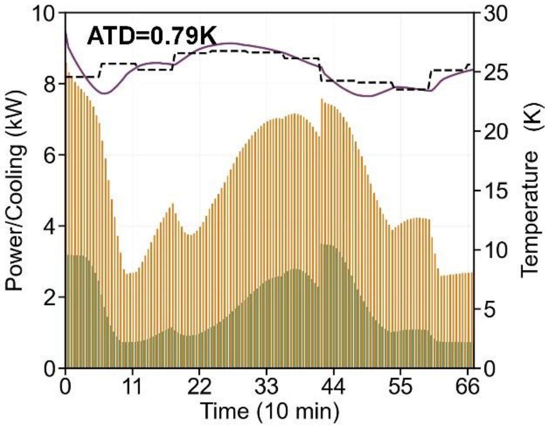

(e) Physical based PID control

Figure 9. Indoor comfort and energy consumption profiles from 8:00 to 18:00 under MPC controllers based on different models and a baseline PID controller. (The purple line represents the indoor temperature trajectory, while the black dashed line indicates the setpoint. The orange and green bars denote the cooling capacity and compressor power consumption, respectively.)

4. Conclusions

In order to address the trade-off between modeling accuracy and computational efficiency in building HVAC control, a novel multi-scale physics-data fusion (Ms-PDF) framework is applied to the VSHP system. Therefore, to advance intelligent building operations, a digital twin driven by a control-oriented state physics-informed neural network (CS-PINN) is integrated with a building thermal model. This hybrid approach supports short-term demand response MPC strategies, ensuring interpretability and scalability. From the obtained results, the conclusions can be drawn as follows:

- Comparative analysis reveals that the proposed Ms-PDF modeling platform achieves an average relative error of only 1.1% in system-level simulations, and the digital twin achieves a prediction accuracy of up to 99.3% for key performance indicators like COP.
- With the developed MPC strategy, energy consumption and comfort-violation rate are reduced by 5.6%~20.7% and 28%~51%, respectively, compared to conventional PID and data-driven baselines.
- Performance analysis indicates that the CS-PINN-based controller demonstrates superior robustness under real operating conditions, maintaining stable temperature tracking where purely data-driven models exhibit significant fluctuations and bias.

The primary barrier is the requirement for relatively accurate component-level specifications to initialize the PINN structure. High-frequency sensor noise can also impact real-time performance. For the future work, we aim to incorporate uncertainty quantification to handle stochastic disturbances (e.g., weather forecast errors) and explore transfer learning to reduce the initial data requirement for new buildings.

Nomenclature

A	Node-edge incidence matrix	*R*	Mass flow rate vector (-)

C	Loop matrix	T	Temperature (°C)
COP	Coefficient of Performance	u	Control input vector
d	External disturbance vector	V	Air volume flow rate (m^3/h)
Fz	Compressor frequency (Hz)	x	System state vector
H	Specific enthalpy vector of nodes	y	Model output vector
h	Refrigerant enthalpy (J/kg)	***Subscript***	
J	Cost function	comp	Compressor
M	Total refrigerant charge (kg)	c	Condenser
m_r	Refrigerant mass flow rate (kg/s)	e	Evaporator
N	Number of nodes/edges	I	Inlet
p	Pressure vector (kPa)	i	node
P	Compressor power (kW)	j	edge
PMV	Predicted Mean Vote (-)	O	Outlet
Q	Cooling capacity (kW)		

Acknowledgements

This work was supported by the National Natural Science Foundation of China (No. 52076085) and the program for HUST Academic Frontier Youth Team (No.2019QYTD10).

References

[1]. Bahramian M, Yetilmezsoy K. Life cycle assessment of the building industry: An overview of two decades of research (1995–2018). *Energy and buildings* 2020;**219**:109917.

[2]. Zhao Y, Li T, Zhang X, Zhang C. Artificial intelligence-based fault detection and diagnosis methods for building energy systems: Advantages, challenges and the future. *Renewable and Sustainable Energy Reviews* 2019;**109**:85-101.

[3]. Hu G, You F. An AI framework integrating physics-informed neural network with predictive control for energy-efficient food production in the built environment. *Applied Energy* 2023;**348**:121450.

[4]. Du Y., Zhao T., Lin J., Wu Y., Wang C., Wu J. An advanced moving-boundary method for the dynamic simulation of split heat pump system under start-up process. *Applied Energy* 2025;**388**:125673.

[5]. Guo Y, Shao S, Geng X, Li H, Wang Z, Akkurt N. A data-driven evaluating method on the defrosting effect of the air source heat pump system in Beijing. *Applied Thermal Engineering* 2023;**235**:121377.

[6]. Chen Q, Li N, Feng W. Model predictive control optimization for rapid response and energy efficiency based on the state-space model of a radiant floor heating system. *Energy and Buildings* 2021;**238**:110832.

[7]. Dou Y, Xu B, Jiang P, Wang X, Zheng, X, Yan Y, Du X. A dual-layer modelling method for characterizing and optimizing the energy flexibility of building heating systems. *Applied Thermal Engineering* 2025;**271**:126312.

[8]. Liang X., Liu Y., Chen S., Li X., Jin X., Du Z. Physics-informed neural network for chiller plant optimal control with structure-type and trend-type prior knowledge. *Applied Energy* 2025;**390**:125857.

[9]. Evens M., Arteconi A. Heat pump digital twin: An accurate neural network model for heat pump behaviour prediction. *Applied Energy* 2025;**378**:124816.

[10]. Guo S., Wei Z., Yin Y., Zhai X. A physics-guided RNN-KAN for multi-step prediction of heat pump operation states. *Energy* 2025;**320**:135108.